Particle Image Velocimetry Measurements of the Flow over Barnacles in a Turbulent Boundary Layer

Julio M. Barros [1*], Elizabeth A. Murphy[2], Michael P. Schultz[3]
1: Dept. of Mechanical Engineering, United States Naval Academy, USA
2: Dept. of Environmental Sciences, University of Virginia, USA
3: Dept. of Naval Architecture and Ocean Engineering, United States Naval Academy, USA
* Corresponding author: barros@usna.edu

Keywords: PIV application, Barnacles, Drag, Biofouling

ABSTRACT

Barnacles are suspension-feeding crustaceans found in saline waters. Past research has focused on the hydrodynamics of larvae settlement and recruitment. These fouling organisms can grow on the hull of marine ships, thus having a significant impact on their performance. The presence of barnacles dramatically increases the frictional drag and consequently has drastic negative economic implications. High-resolution Particle-Image Velocimetry is used to measure the flow over barnacles immersed into a turbulent boundary layer. Two configurations were investigated - *i*) single-barnacle configuration and *ii*) a regular, staggered array of barnacles. Mean flow quantities between these two configurations are strikingly similar when visualizing the flow around an individual element. Quadrant analysis revealed important structural behavior, especially when only considering the strongest Reynolds shear stress events. These events are likely linked to contribute to both larval settlement and waste removal.

1. Introduction

Barnacles are common intertidal and fouling organisms found on hard substrates in marine systems, such as rocky shores and ship hulls. Barnacle fouling has huge consequences on ship performance due to the addition of roughness to the ship surface. This roughness dramatically increases the frictional drag on a ship, increasing fuel use and shipping costs [20, 21]. The integrated frictional drag induced by barnacle fouling has been measured, as have the hydrodynamic forces on individual barnacles [22]. However, detailed analysis of the turbulence structure around individual barnacles and groups of barnacles is lacking. Understanding the flow around these fouling communities will provide insight regarding the roughness scales that contribute significantly to the drag, with the aim of developing predictive models of drag increase due to specific fouling communities. The present work takes a first step in investigating the interaction of an isolated barnacle and a regular, staggered array of barnacles with a turbulent boundary layer flow.

The data presented here are also relevant from an ecological perspective. Flow structures near colonies of sessile marine organisms impact the ability of the colony to reproduce and recruit larvae, encounter food, and remove waste [6, 25]. Barnacles form dense aggregates on available substrates, with intense competition for space within the colony [15]. Barnacles feed on plankton by waving a cirral basket (a rake-like appendage used for suspension feeding) in the water column. Past research has focused on the hydrodynamics of larvae settlement and recruitment [8, 27] and of particle capture [14, 17]. For example, higher shear stresses and turbulent momentum transport can make it more likely for settled larva to be swept away, but some amount of enhanced turbulence and shear stresses due to the topography of the fouling community is needed to induce settlement behavior [12]. Researchers studying other species of benthic organisms have investigated the effects of aggregations on hydrodynamics above the colony, often with a focus on feeding [7]. Aggregates of individuals increase the surface roughness, and therefore the shear stresses and turbulence above the bed, resulting in increased mass transport to the bed. Vortices shed off of upstream individuals can result in higher food encounter rates in downstream individuals [23]. Groups of organisms are often exposed to less severe forces from currents and waves than a solitary individual would be [9]. Conversely, densely packed colonies can result in skimming flow over the tops of the individuals, with stagnant water within the colony [23].

Here we present detailed, high resolution PIV data around an individual barnacle and an array of barnacles, with the aim of better understanding their effect on the turbulent flow field. Specifically, the location of turbulent kinetic energy production and wake formation is examined, as well as regions of enhanced turbulent ejection and sweep behavior. That is, where high momentum fluid from further up in the boundary layer sweeps down into the lower boundary layer and along the bed, and is ejected back out. This turbulent behavior is important to sessile organisms, especially over colonies where gradients of food and oxygen are often present due to depletion near the bed, because these fluid structures can entrain fluid with higher concentrations of desired substances and deliver it to the organisms. The Reynolds shear stress due to these turbulence structures also increases skin friction resulting in higher drag [13]. Therefore, the present results have implications for both the effects of barnacle fouling on ship drag as well as barnacle ecology.

2. Experiments

Experiments were conducted in a water tunnel designed for detailed boundary-layer measurements. The test section was 2 m long, 0.2 m wide, and nominally 0.1 m high. The bottom wall was a flat plate which served as the test wall. The upper wall was adjustable and set for a

zero streamwise pressure gradient with a free-stream velocity, U_e, of ~ 1.25 m/s for all cases. The acceleration parameter, defined as

$$K = \frac{\nu}{U_e^2} \frac{\mathrm{d}Ue}{\mathrm{d}x}$$

was less than 5×10^{-9}. The upper wall and sidewalls provided optical access. The boundary layer was tripped near the leading edge with a 0.8 mm diameter wire, fixing the location of transition and ensuring a turbulent boundary layer. Velocity measurements showed that a core flow remained to the downstream end of the test section. Flow was supplied to the test section from a 1900 L cylindrical tank. Water was drawn from the tank to two variable-speed, 7.5 kW pumps operating in parallel and then sent to a flow-conditioning section consisting of a diffuser containing perforated plates, a honeycomb, three screens and a three-dimensional contraction. The test section followed the contraction. The free-stream turbulence level was less than 0.5%. Water exited the test section through a perforated plate emptying into the cylindrical tank. The test fluid was filtered and deaerated water. A chiller was used to keep the water temperature constant to within 1 K during all tests.

2.1 Single-Barnacle Setup

The barnacle model was obtained by 3d-scans of a real organism (*Amphibalanus amphitrite*), which then was 3d-printed and further replicated by a mold/cast technique. The barnacle was affixed to the smooth wall at a location ~ 1.5 m downstream of the trip wire. The height of the barnacle is 10mm, and the major and minor axis dimensions are 25 mm and 23 mm, respectively. The Reynolds number based on the momentum thickness is Re_θ ~ 5500, and the boundary-layer thickness is δ ~ 34.0 mm.

Tab.1 Summary of the important flow parameters

Configuration	Re_θ	$U_e\,[m/s]$	$\delta\,[mm]$	$h\,[mm]$
Single-barnacle	5518	1.24	34.24	10
Barnacle-array	9416	1.27	47.96	4

2.2. Barnacle Array Setup

The same barnacle model was used to create the array. The barnacles were arranged in a staggered fashion, where the planform roughness density was set to $\lambda_P = 0.20$. Figure 1 illustrates the employed barnacle arrangement. That is, the barnacles were spaced from one another by one

barnacle dimension in the $x – y$ direction. A single tile of the aforementioned arrangement was generated in a CAD software (Solidworks), with dimension of 155.81mm x 203.2mm ($x – y$), where the barnacle models were placed on top of a 2mm baseplate. It is worth mentioning that the barnacle model was scaled down to have a nominal height of h = 4mm so that their crests were located in the log-layer region of the flow (behaving as roughness elements and not flow over blunt obstacles). A total of eight tiles were 3d-printed, which were then affixed onto an acrylic plate, thus providing ~ 1.2m of fetch in the streamwise direction.
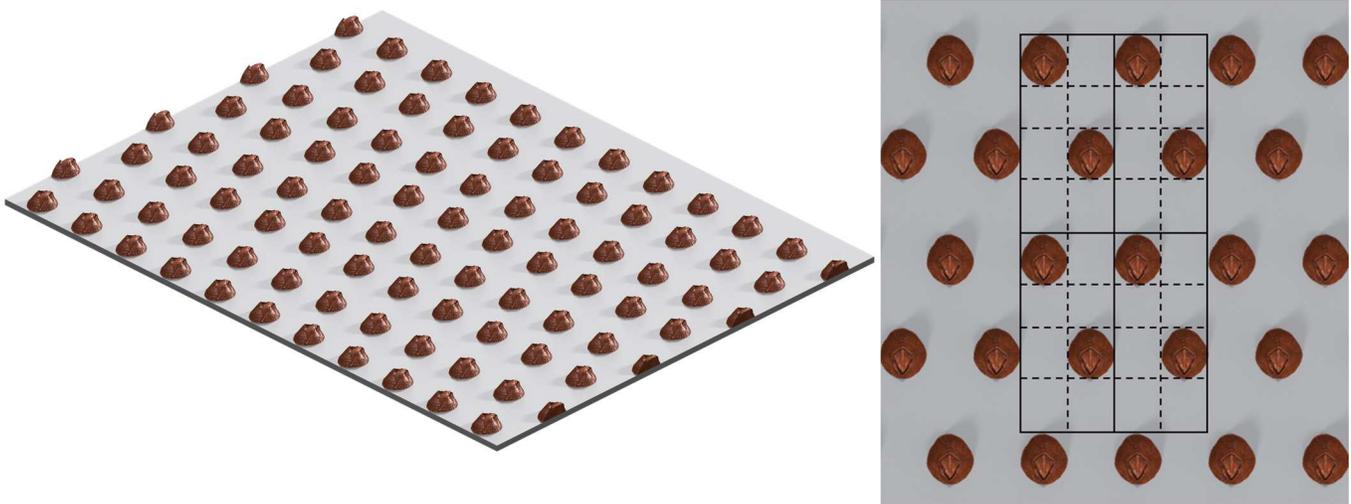

Fig. 1 Illustration of the barnacle array arrangement employed. Left panel shows the generated tile, and the right panel highlights the staggered arrangement, where the black solid rectangle boxes demarcate the repeating barnacle pattern.

2.3 Particle Image Velocimetry Setup

Particle image velocimetry (PIV) was used to capture the flow field for both experiments in the streamwise - wall-normal ($x − y$) plane. The system consisted of one $6.6k \times 4.4k$ pixel, 12 bit frame straddle CCD camera (TSI 29MP) coupled with a 190 mJ per pulse, dual-cavity pulsed Nd:YAG laser (Quantel). A 0.3 mm thick laser lightsheet was formed by a spherical-cylindrical lens configuration. The flow was seeded with 2 μm silver coated glass-sphere particles, and all measurements were performed ~ 1.5 m downstream of the trip wire at the entrance of the test section. The timing of the system was controlled by a synchronizer unit with 1ns resolution. Careful consideration was taken when defining the time-delay, dt, between the image-pairs. Due to the complex flow topology behind the barnacles, the dt was chosen such that all the resolvable flow recirculation displacements were approximately 4px. The time-delayed images were interrogated using a recursive two-frame cross-correlation methodology, with a final pass of 24^2 pixels for the single-barnacle configuration, and 32^2 pixels for the array-configuration, all with

50% overlap to satisfy the Nyquist sampling criterion (Insight 4G version 11). Statistical validation tools were employed to identify and replace erroneous vectors, including the replacement with displacement assessed from secondary peaks from the correlation map identified during the interrogation process. All the instantaneous field were then low-pass filtered with a narrow Gaussian filter to remove high-frequency noise. On average, the number of interpolated vectors was between 1-2%. For each aforementioned experiment, 4000 statistically independent instantaneous velocity fields were acquired. The final field-of-view (FOV) for the single-barnacle configuration was $\sim 6h \times 4.5h$, where h = 10 mm is the barnacle height, and the final grid resolution was 134μm, and for the array configuration the FOV was $\sim 25h \times 15h$, where h = 4 mm is the barnacle height, and the final grid resolution was 246μm.

3. Results

3.1. Single-Barnacle Configuration

3.1.1. Mean Statistics

Figure 2a) shows the outer-scaled mean streamwise velocity field ($\langle U \rangle / U_e$). Both the streamwise and wall-normal axis were normalized by the height of the barnacle ($h = 10.0$ mm). For the single barnacle configuration, the mean streamwise velocity (fig. 2a) accelerates at the top of the barnacle ($y/h > 1.0$), causing flow separation and creating a wake region downstream of the barnacle. The flow reattaches at x/h = 3.6 (about $1.3h$ downstream of the barnacle's lee side). Additionally, the momentum deficit caused by the presence of the barnacle extends well beyond the measured field-of-view ($x/h > 6$).
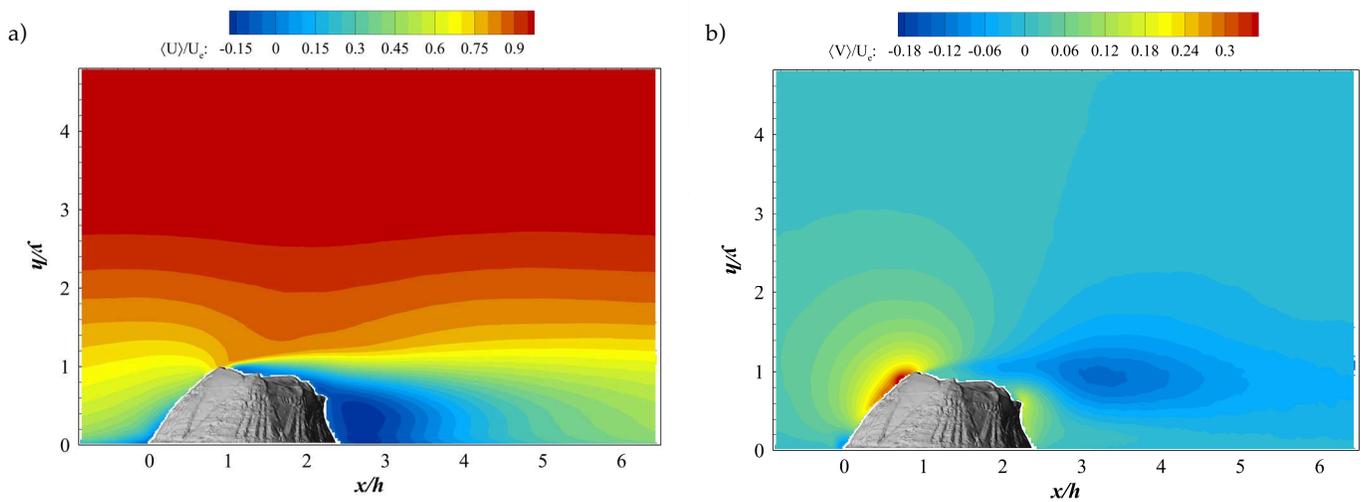

Fig. 2 Streamwise mean velocity field, (a), and wall-normal mean velocity field, (b) for the single-barnacle configuration. The mean velocities were normalized using the free-stream velocity, U_e and the axes with the barnacle height, h.

In order to highlight more clearly the impact of the barnacle presence in the flow, fig. 2b) presents the outer-scaled mean wall-normal velocity field ($\langle V \rangle / U_e$). As can be seen, the flow sharply changes direction ($\langle V \rangle > 0$) at the leading edge of the barnacle. As expected, the wake region is characterized by a strong negative mean wall-normal velocity (about 10% of U_e) that extends to $\sim x/h = 5$, and positive, upward flow ($\langle V \rangle > 0$) closely adjacent to the barnacle's lee side. It is worth pointing out that the negative contour levels of $\langle V \rangle$ seem to be largely parallel to the wall. Figure 3a) presents the outer-scaled turbulent-kinetic-energy ($TKE = 1/2\langle u'^2 + v'^2 \rangle$). Due to the flow separation behind the single barnacle-configuration (fig. 3a), a region of enhanced TKE is observed that extends well over $x/h = 6$. It is worth pointing out that the initiation of the enhanced TKE starts at the sharp leading edge of the barnacle shell which is present in most balanoid barnacles.

Similar behavior is observed for the Reynolds shear stress (RSS, $\langle u'v' \rangle$) in fig. 3b), where a region of enhanced RSS is observed at the shear layer, due to flow separation downstream of the barnacle, which extends well beyond $x/h = 6$.
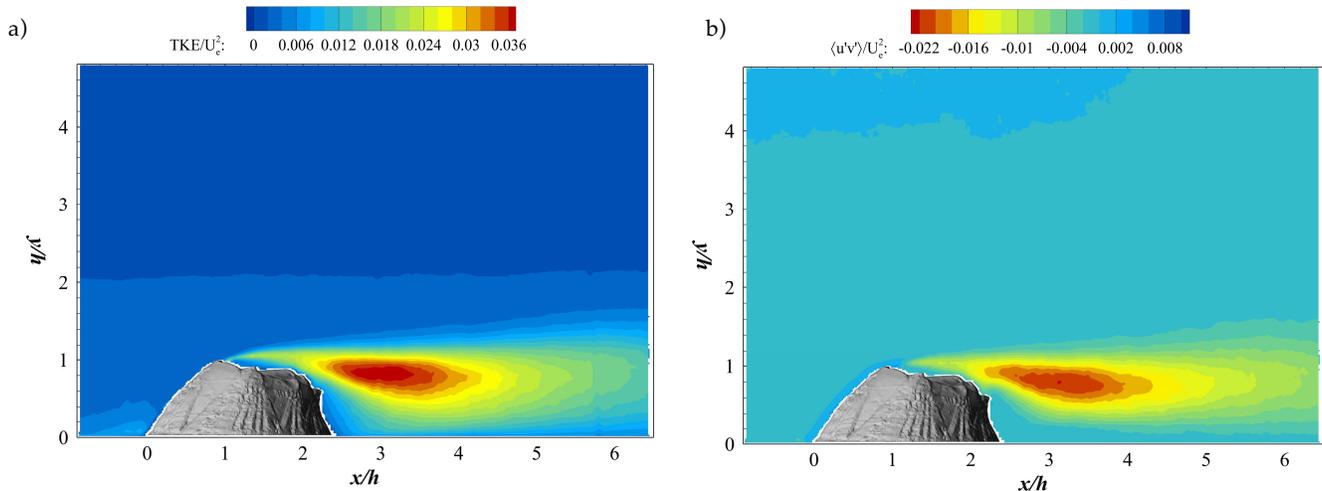

Fig. 3 Turbulent kinetic energy ($TKE = 1/2\langle u'^2 + v'^2 \rangle$; a) and the Reynolds shear stress (RSS, $\langle u'v' \rangle$, b) for the single-barnacle configuration. The mean quantities were normalized using the free-stream velocity, U_e, and the axes with the barnacle height, h.

3.1.2. Quadrant Analysis

To further explore the overall RSS behavior of the flow structures, quadrant analysis was employed. The instantaneous $u'v'$ events that generate the RSS field shown in fig. 3b) are formed by different combinations of u' and v' instantaneous events. More specifically, depending upon the combination, these events will lie in one of the four quadrants of the $u' - v'$ plane. It is well

known, and has also become an important nomenclature in wall-bounded flows, that negative contributions to the $\langle u'v' \rangle$ are termed ejections, $Q_2: u' < 0, v' > 0$, and sweeps, $Q_4: u' > 0, v' < 0$, events. Positive contributions to the $\langle u'v' \rangle$ are known as inward, $Q_3: u' < 0, v' < 0$, and outward, $Q_1: u' > 0, v' > 0$ interactions. It is well-appreciated that ejection and sweep events dominate, in a mean sense, over inward and outward interactions as reflected in the negative sign of $\langle u'v' \rangle$ throughout the boundary layer, which is observed in fig. 3b).

The quadrant decomposition of instantaneous $u'v'$ events is given by

$$\langle u'v' \rangle_Q(x, y; H) = \sum_{n=1}^{N} u'(x, y)v'(x, y)I_Q(x, y; H), (1)$$

where H is the hyperbolic hole size and N is the total number of samples. It should be noted that the averaging reflected in the summation of eqn. (1) is only through the ensemble of velocity fields (hence, $N = 4\,000$) so as to maintain the streamwise and wall-normal dependence of the decomposition and thus facilitate identification of spatial heterogeneity in the various quadrant contributions. The indicator function, $I_Q(x, y)$ in eqn. (1) is defined as

$$I_Q(x, y; H) = \begin{cases} 1, when \ |u'(x, y)v'(x, y)|_Q \geq T(x, y) \\ 0, otherwise, \end{cases}$$

where $T(x, y)$ is a threshold allowing one to consider different strengths of the instantaneous RSS events that contribute to the mean RSS. This threshold is defined as

$$T(x, y) = H\sigma_u(x, y)\sigma_v(x, y),$$

where $\sigma_u(x, y) = \sqrt{\langle u'^2 \rangle}$ and $\sigma_v(x, y) = \sqrt{\langle v'^2 \rangle}$ are the root-mean-square (RMS) streamwise and wall–normal velocities, respectively, which vary in both x and y (thus justifying the spatial dependence of T).

A hyperbolic hole size of $H = 0$ is considered first, meaning all $u'v'$ events contributing to the mean RSS in fig. 3b) are considered in the analysis. For brevity, only Q_2 and Q_4 is presented herein. It is important to remark, however, that the contribution of both inward and outward interaction are negligible (approximately an order of magnitude smaller), regardless of the presence of the barnacle, meaning that these events do not play a significant role in the overall development of RSS.

Figure 4 presents the contour maps of Q_2 and Q_4 for a hyperbolic hole size of $H = 0$ for the single-barnacle configuration. It can be seen that nearly equal contribution of sweeps and ejections is observed in both quadrants. In addition, the core of highest Q_2 and Q_4 content extends to $x/h = 4$. However, they exhibit some significant differences. For example, where Q_2 events show an inclination of the core that tends to move away from the wall, the Q_4 events exhibit the opposite tendency up to $x/h = 4$, where it tends to move parallel to the wall thereafter.
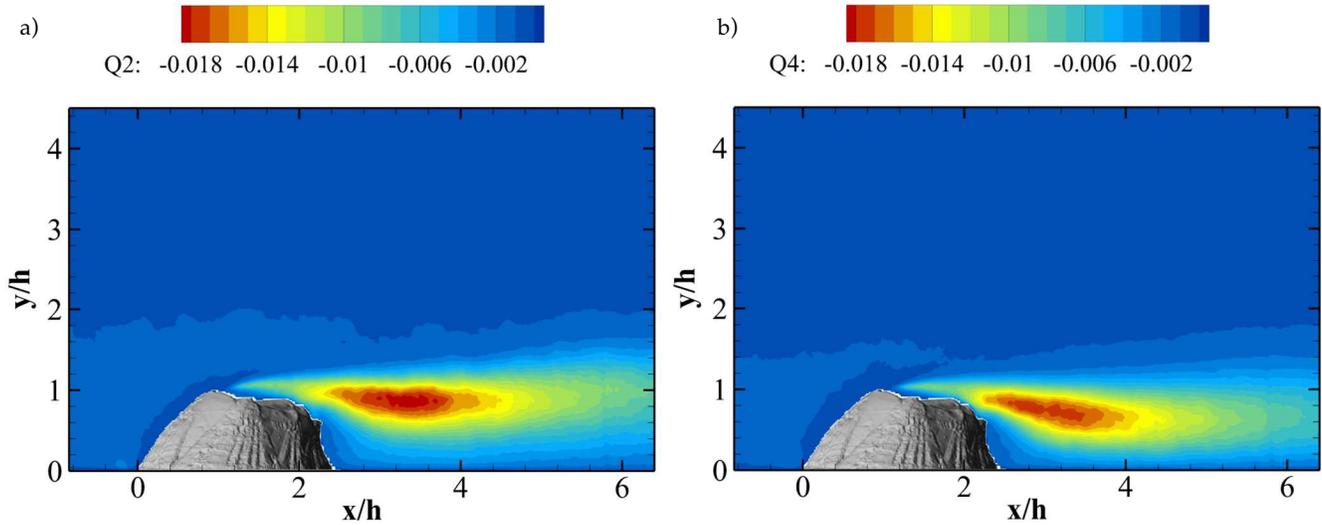

Fig. 4 *Contour maps of ejections,* Q_2; $\langle u'v' \rangle_2$ *and sweeps,* Q_4; $\langle u'v' \rangle_4$, *for single-barnacle configuration, using H=0. The axes are normalized by the barnacle height, h.*

In order to assess the role of the more intense RSS events in these trends, quadrant analysis with a hyperbolic hole size of $H = 4$ is presented in fig. 5. Interestingly, the aforementioned differences are now more apparent. Similar to the results for $H = 0$ (fig. 3), Q_2 events show an inclination of the core that moves away from the wall, whereas the Q_4 events exhibit the opposite tendency. Although these events show similar tendencies when compared with $H = 0$, Q_2 events are more dominant than Q_4 events for the hyperbolic hole size $H = 4$. Comparing these observations with the mean flow data that are presented in fig. 2, the Q_2 events appear to be related to the shear layer that emanates from the leading edge of the barnacle shell and extends downstream. The Q_4 events on the other hand coincide with the top of the separation bubble located in the lee of the barnacle. It is well known that Q_2 events transport low speed fluid way from the wall, whereas Q_4 events transport high momentum fluid towards the wall. In fact, these events likely contribute significantly to important processes in larval dispersal and settlement, food supply, and waste removal. More specifically, Q_4 events may enhance food supply and larval settlement by increasing the instantaneous turbulent mass flux toward the wall [27, 10]. In contrast, Q_2 events

may aid in larval dispersal and waste removal by increasing the instantaneous turbulent mass flux into the bulk flow [6, 18].

Patterns of RSS and turbulent burst and sweep behavior have been shown to influence larval settlement behavior. For example, settling oyster larvae pick up hydrodynamic cues and preferentially settle in locations with high RSS and TKE above the bed [27] and low RSS and TKE at the bed. Areas where high momentum fluid is carried towards the bed, while TKE and RSS are lower at the bed, are likely to transport more larvae to the colony while maintaining settlement due to lower hydrodynamic forces on the larvae after settlement.
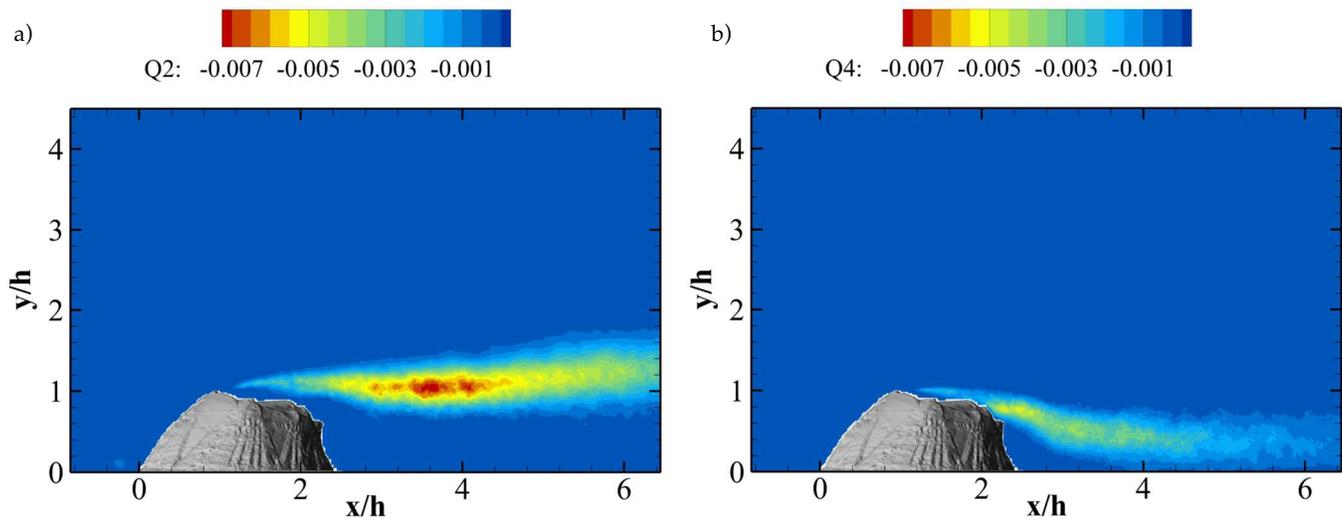

Fig. 5 Contour maps of ejections, Q_2; $\langle u'v'\rangle_2$ and sweeps, Q_4; $\langle u'v'\rangle_4$, for single-barnacle configuration, using $H = 4$. The axes are normalized by the barnacle height, h.

3.2. Barnacle Array Configuration

3.2.1 Mean Statistics

Figure 6 presents both the mean streamwise velocity, $\langle U\rangle$ and the mean wall-normal velocity, $\langle V\rangle$, normalized by the free-stream velocity, U_e. It is worth pointing out once more that these measurements were taken in the streamwise-wall-normal direction ($x – y$) at the centerline of the water tunnel. Focusing upon the region above the barnacle elements ($y/h > 2$), both the mean streamwise and wall-normal velocities have the characteristics of a fully-developed rough-wall flow, where the streamwise velocity contours are largely parallel to the bottom wall and the wall-normal velocity contours values are nearly zero. Conversely, the flow immediately above and within the barnacle elements ($y/h < 2$) shows significant spatial heterogeneity, especially for $\langle V\rangle$, where these heterogeneities spread more into the boundary layer. It is quite clear to visualize the

location of the barnacle elements that are in the measurement plane (from left to right they are the first, third and fifth blank spaces, whereas the second, fourth and sixth blank areas correspond to the elements outside the measurement region that blocked the field-of-view), based on the mean flow pattern around the elements. Focusing upon a given barnacle element (say, at $x/h \sim 10$), interestingly, the mean flow behavior is quite similar to the one for the isolated single-barnacle configuration (fig. 2) for both the mean streamwise and wall-normal velocities. However, as expected, the magnitude between these two configurations are different.
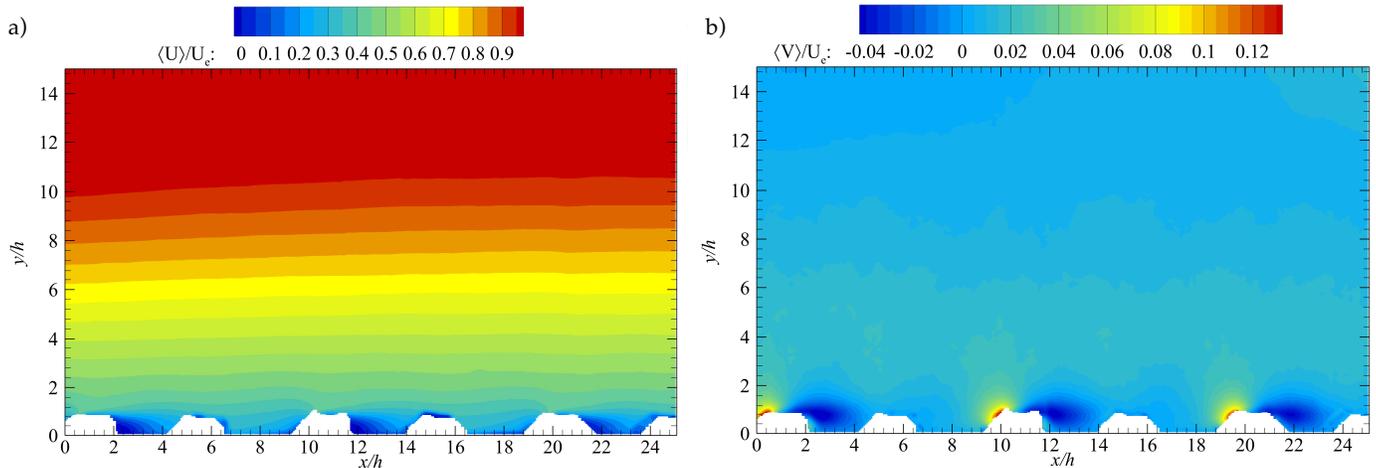

Fig. 6 *Streamwise mean velocity, (a), and wall-normal mean velocity fields, (b), for the barnacle-array configuration. The mean velocities were normalized using the free-stream velocity, U_e and the axes with the barnacle height, h.*

Figure 7 shows the *TKE* and the *RSS*, normalized by the free-stream velocity, U_e. Similar to the mean velocity behavior seen in figure 6 in the region above the barnacle elements ($y/h > 2$), both *TKE* and *RSS* display the characteristics of a fully-developed rough-wall turbulent flow. Moreover, the overall *TKE* and *RSS* behavior at a given barnacle element is strikingly similar to the behavior seen in the single-barnacle configuration (fig. 3; again, the magnitude between these two configurations are also different). Looking at the figure 7a), the enhanced *TKE* regions seem to initiate at the leading edge of the top of the barnacle shell and extend about two barnacle heights downstream.

Additionally, a careful examination of the contours between $y/h = 1 - 2$ in fig. 7a) reveals that these regions of enhanced *TKE* (demarcated by the yellow contours) seem to possess an inclination angle that extends these regions far from the wall and are adjacent to regions of less *TKE* content (demarcated by light blue contours to light green) that seem to initiate just downstream of the position where the barnacles outside the measurement plane are located. Moreover, these regions of less *TKE* content seem to possess a slight inclination angle as well. This pattern can be seen

throughout the entire field-of-view and are likely linked to the relatively sparse planform density of the barnacles coupled with their organized arrangement in this work. A very similar behavior to the *TKE* is also seen on the RSS in figure 7b), where regions of enhanced *RSS* extend about $2h$ downstream of the barnacle elements, and the presence regions of less *RSS* content with a slight inclination angle extend away from the wall.
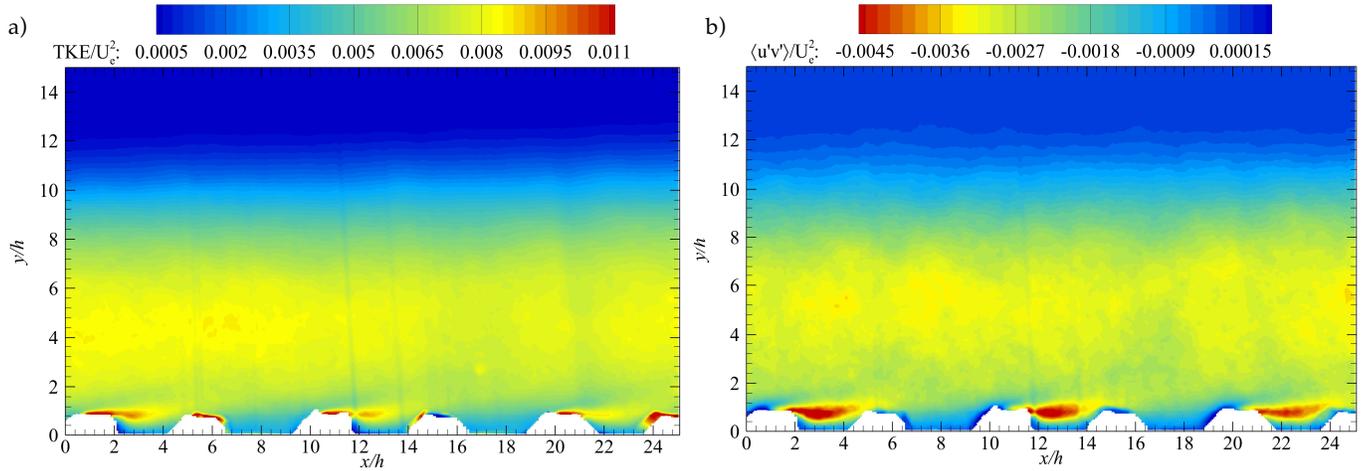

Fig. 7 Turbulent kinetic energy (TKE = 1/2⟨u′² + v′²⟩; a) and the Reynolds shear stress (RSS, ⟨u′v′⟩; b) for the barnacle-array configuration. The mean quantities were normalized using the free-stream velocity, U_e, and the axes with the barnacle height, h.

3.2.2 Quadrant Analysis

Quadrant analysis was also employed for the barnacle array configuration, using the same procedure described for the single-barnacle configuration, to investigate the role the different quadrants have on the overall RSS.
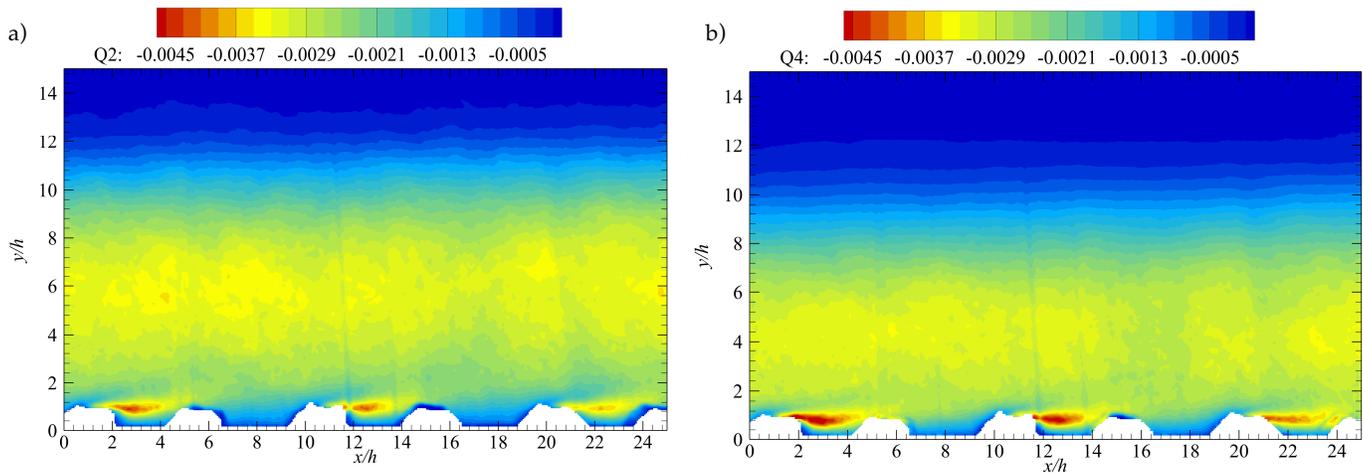

Fig.8 Contour maps of ejections, Q_2; ⟨u′v′⟩$_2$ and sweeps, Q_4; ⟨u′v′⟩$_4$, for barnacle-array configuration, using H = 0. The axes are normalized by the barnacle height, h.

Again, it is important to note that the contribution of both inward and outward interactions are negligible (approximately one order of magnitude smaller), and, for brevity, are not shown here. Figure 8 shows the contour maps of Q_2 and Q_4 for a hyperbolic hole size of $H = 0$. Focusing upon the region around a given barnacle element, it can be seen that Q_4 events are more dominant than Q_2 events. Regardless of the difference in magnitude, the core of highest Q_2 and Q_4 events extend about $2h$ downstream for the barnacle elements in the measurement plane. The aforementioned patterns of low and enhanced RSS content seen in fig. 7b) are more apparent when visualizing the different quadrant events (fig. 8), and these patterns are more strongly present in Q_2. However, Q_4 seems to exhibit the same behavior to some extent. It is worth pointing out that the overall structure of the Q_2 and Q_4 between the single-barnacle and the array configuration are largely similar.

In order to investigate the contribution of the strongest $u'v'$ events to the overall RSS, quadrant analysis with a hyperbolic hole of $H = 4$ is presented in fig. 9. Significant differences between Q_2 and Q_4 can be readily seen. The aforementioned patterns of low and enhanced RSS content (fig. 7b; also observed in fig. 8a) are reveled when considering the strongest Q_2 events shown in fig. 9a). Interestingly, this pattern does not seem to occur when only strong Q_4 are considered, which is shown in fig. 9b). In addition, similarly to what was observed for $H = 0$ in fig. 8, the cores of highest Q_2 events are inclined away from the wall, whereas the cores of highest Q_4 events are inclined towards the wall. Furthermore, Q_4 events are more dominant than Q_2 events.
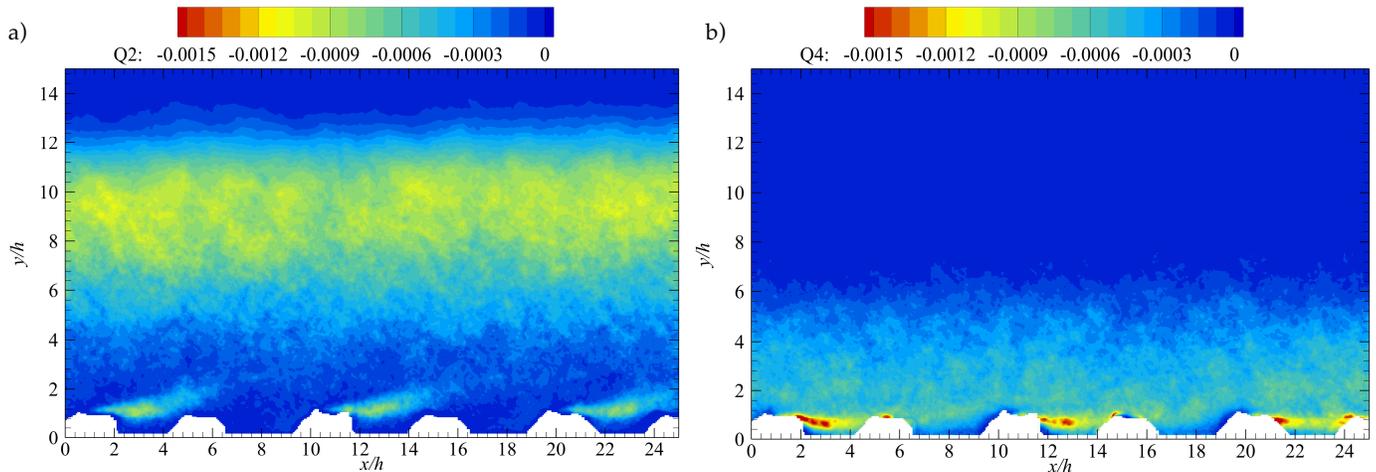

Fig. 9 Contour maps of ejections, Q_2; $\langle u'v'\rangle_2$ and sweeps, Q_4; $\langle u'v'\rangle_4$, for barnacle-array configuration, using $H = 4$. The axes are normalized by the barnacle height, h.

It is worth mentioning again that Q_2 events transport low speed fluid away from the wall, whereas Q_4 events transport high momentum fluid towards the wall. Due to the similar nature of the

overall mean flow structure and *RSS* patterns between the single-barnacle and array configuration, once more, these events are likely linked for contributing significantly towards important processes in larval dispersal and settlement, food supply, and waste removal [6, 10, 18, 27]. However, the chosen barnacle arrangement enhances the generation of Q_4 events. In a biological and ecological context, this aspect likely contributes to enhancing larval settlement and food supply in the near wall region.

Although the measurements performed in this work do not provide such information, it can be conjectured, however, that the organized arrangement of the barnacle elements could trigger preferential pathways for the low- and high-momentum regions and thus triggering the so called low- and high-momentum pathways (LMP and HMP, respectively), as seen by Barros & Christensen (2014)[5] and others [4, 16, 24]. The main implication is that these mean pathways generate heterogeneities in the spanwise direction on all the mean turbulent quantities, which ultimately creates a variation of the skin friction, C_f, in the spanwise direction [28]. Measurements in the streamwise-spanwise plane ($x – z$) could help reveal the presence of these pathways.

4. Summary

The high resolution boundary layer flow data acquired herein provides important information on turbulent momentum transport over individual barnacles and barnacle colonies in the form of an organized barnacle arrangement. The mean flow structures around the single-barnacle configuration and an individual barnacle element in the array configuration are strikingly similar. This phenomenon might be linked to the chosen regular, staggered arrangement coupled with the relatively sparse planform density of the barnacles tested here. However, as expected, the flow above the barnacle array configuration is quite different, where it displays fully developed rough-wall characteristics.

The data presented here show that the biology and ecology of barnacle communities, e.g. competition for space and food leading to aggregate spacing, have consequences for the boundary layer flow structure over the colony, which, in turn, likely impacts the performance of marine vessels. From a biological perspective, the location and magnitude of sweep and ejection events has implications for the delivery of larvae and food to the barnacle individual or colony and removal of waste products from the barnacle colony. Together, the data presented herein indicate that there is significant feedback between the barnacle colony structure and the colony hydrodynamics.

Acknowledgements

5. References

[1] Adrian, R., Christensen, K., and Liu, Z.-C. *Analysis and interpretation of instantaneous turbulent velocity fields.* Experiments in Fluids 29, 3 (2000), 275–290.

[2] Adrian, R. J. *Twenty years of particle image velocimetry.* Experiments in Fluids 39, 2 (2005), 159–169.

[3] Adrian, R. J., and Westerweel, J. *Particle image velocimetry.* No. 30. Cambridge University Press, 2011.

[4] Anderson, W., Barros, J.M., Christensen, K.T. and Awasthi, A., 2015. *Numerical and experimental study of mechanisms responsible for turbulent secondary flows in boundary layer flows over spanwise heterogeneous roughness.* Journal of Fluid Mechanics, 768, pp.316-347.

[5] Barros, J.M. and Christensen, K.T., 2014. *Observations of turbulent secondary flows in a rough-wall boundary layer.* Journal of Fluid Mechanics, 748, p.R1.

[6] Burks, R. L., Tuchman, N. C., Call, C. A., and Marsden, J. E. *Colonial aggregates: effects of spatial position on zebra mussel responses to vertical gradients in interstitial water quality.* Journal of the North American Benthological Society 21, 1 (2002), 64–75.

[7] Crimaldi, J. P., Koseff, J. R., and Monismith, S. G. *A mixing-length formulation for the turbulent prandtl number in wall-bounded flows with bed roughness and elevated scalar sources.* Physics of Fluids (1994-present) 18, 9 (2006), 095102.

[8] Crimaldi, J. P., Thompson, J. K., Rosman, J. H., Lowe, R. J., and Koseff, J. R. *Hydrodynamics of larval settlement: The influence of turbulent stress events at potential recruitment sites.* Limnology and Oceanography 47, 4 (2002), 1137–1151.

[9] Denny, M. W. *Wave forces on intertidal organisms: A case study.* Limnology and Oceanography 30, 6 (1985), 1171–1187.

[10] Hendriks, I. E., Van Duren, L. A., and Herman, P. M. *Turbulence levels in a flume compared to the field: implications for larval settlement studies.* Journal of Sea Research 55, 1 (2006), 15–29.

[11] Keane, R. D., And Adrian, R. J. *Theory of cross-correlation analysis of PIV images.* Applied Scientific Research 49, 3 (1992), 191–215.

[12] Koehl, M. *Mini review: hydrodynamics of larval settlement into fouling communities.* Biofouling 23, 5 (2007), 357–368.

[13] Kravchenko, A. G., Choi, H., and Moin, P. *On the relation of near-wall streamwise vortices to wall skin friction in turbulent boundary layers.* Physics of Fluids A: Fluid Dynamics (1989-1993) 5, 12 (1993), 3307–3309.

[14] Li, N. K., and Denny, M. W. *Limits to phenotypic plasticity: flow effects on barnacle feeding appendages.* The Biological Bulletin 206, 3 (2004), 121–124.

[15] Marchinko, K. B., and Palmer, A. R. *Feeding in flow extremes: dependence of cirrus form on wave-exposure in four barnacle species.* Zoology 106, 2 (2003), 127–141.

[16] Nugroho, B., Hutchins, N. and Monty, J.P., 2013. *Large-scale spanwise periodicity in a turbulent boundary layer induced by highly ordered and directional surface roughness.* International Journal of Heat and Fluid Flow, 41, pp.90-102.

[17] Pullen, J., and Labarbera, M. *Modes of feeding in aggregations of barnacles and the shape of aggregations.* The Biological Bulletin 181, 3 (1991), 442–452.

[18] Quinn, N. P., and Ackerman, J. D. *Effects of near-bed turbulence on the suspension and settlement of freshwater dreissenid mussel larvae.* Freshwater Biology 59, 3 (2014), 614–629.

[19] Raffel, M., Willert, C. E., Kompenhans, J., et al. *Particle image velocimetry: a practical guide.* Springer, 2013.

[20] Schultz, M., Bendick, J., Holm, E., and Hertel, W. *Economic impact of biofouling on a naval surface ship.* Biofouling 27, 1 (2011), 87–98.

[21] Schultz, M. P. *Frictional resistance of antifouling coating systems.* Journal of Fluids Engineering 126, 6 (2004), 1039–1047.

[22] Schultz, M. P., Kavanagh, C. J., and Swain, G. W. *Hydrodynamic forces on barnacles: Implications on detachment from fouling-release surfaces.* Biofouling 13, 4 (1999), 323–335.

[23] Thomason, J., Hills, J., Clare, A., Neville, A., and Richardson, M. *Hydrodynamic consequences of barnacle colonization.* In Recruitment, Colonization and Physical-Chemical Forcing in Marine Biological Systems. Springer, 1998, pp. 191–201.

[24] Vanderwel, C. and Ganapathisubramani, B., 2015. *Effects of spanwise spacing on large-scale secondary flows in rough-wall turbulent boundary layers.* Journal of Fluid Mechanics, 774, p.R2.

[25] Walters, L. J., and Wethey, D. S. *Settlement, refuges, and adult body form in colonial marine invertebrates: a field experiment.* The Biological Bulletin 180, 1 (1991), 112–118.

[26] Westerweel, J. *Fundamentals of digital particle image velocimetry.* Measurement Science and Technology 8, 12 (1997), 1379.

[27] Whitman, E. R., and Reidenbach, M. A. *Benthic flow environments affect recruitment of crassostrea virginica larvae to an intertidal oyster reef.* Marine Ecology Progress Series 463 (2012), 177–191.

[28] Willingham, D., Anderson, W., Christensen, K.T. and Barros, J.M., 2014. Turbulent boundary layer flow over transverse aerodynamic roughness transitions: Induced mixing and flow characterization. Physics of Fluids (1994-present), 26(2), p.025111.